Precise regulation of monomer reactive sites enhances water permeance and membrane selectivity of polyamide nanofiltration membranes

Ke Jiang,[1] Li Long,[1]* Lu Elfa Peng,[1] Zhe Yang,[1] Wenyu Liu,[1] Dong-Myeong Shin[2] and Chuyang Y. Tang[1] *

[1] Department of Civil Engineering, The University of Hong Kong, Pokfulam, Hong Kong SAR, P. R. China.

[2] Department of Mechanical Engineering, The University of Hong Kong, Pokfulam, Hong Kong SAR, P. R. China.

* Corresponding authors:

Prof. Chuyang Y. Tang, phone: +852 2859 1976, e-mail address: tangc@hku.hk

Dr. Li Long, phone: +852 6740 2649, e-mail address: longli@connect.hku.hk

ABSTRACT

Polyamide structure and chemistry play a critical role in the separation performance of thin film composite (TFC) nanofiltration (NF) membranes. Typically, the polyamide formation is based on the reactive sites on monomers (e.g., amino groups on piperazine (PIP)) during interfacial polymerization (IP). To precisely tailor polyamide properties (e.g., crosslinking degree) and membrane performance, we regulated PIP reactive sites by pH adjustment to vary the dominant species in forms of non-, mono-, and di-protonated PIP. Specifically, at pH values between pK_{a1} (i.e., 5.3) and pK_{a2} (i.e., 9.7), the dominant mono-protonated PIP with relatively fewer non-protonated PIP resulted in reduced crosslinking degree of polyamide. Such reduced crosslinked polyamide exhibited simultaneously improved water permeance and better solute-to-solute selectivity (e.g., $CaCl_2/Na_2SO_4$ and $CaCl_2$/PFOS selectivity), thanks to their looser structure and more negative charge. For example, the membrane NF-pH9, prepared at pH 9, exhibited simultaneously improved water permeance (20.2 L m^{-2} h^{-1} bar^{-1}) and higher $CaCl_2$/PFOS selectivity (12.6). The dominant di-protonated PIP with few non-protonation at pH < pK_{a1} resulted in ineffective crosslinked polyamide with low salt rejection (e.g., 0.9 ± 0.3% of Na_2SO_4). This study investigated a facile strategy to tailor membrane permeance and selectivity by regulating monomer reactive sites, which provides new insights into developing high-performance NF membranes.

TABLE OF CONTENTS

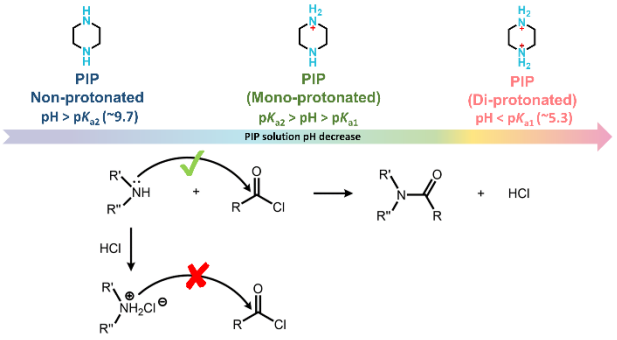

1. INTRODUCTION

Nanofiltration (NF) technology has been extensively applied in a wide range of water treatment scenarios.[1, 2] This technology is generally based on thin film composite (TFC) membranes featuring a semi-aromatic polyamide layer on a porous substrate.[3, 4] The polyamide layer is typically prepared by the interfacial polymerization (IP) between piperazine (PIP) in an aqueous solution and trimesoyl chloride (TMC) in an organic solvent.[5, 6] One essential indicator for NF membrane performance is the solute-to-solute selectivity, which enables selective retention/passage of small molecules and ions. The membrane selectivity is greatly influenced by the structure and chemistry (e.g., pore size and surface charge) of its polyamide layer.[7, 8]

To date, several strategies have been applied to tailor IP for regulating the structure and chemistry of polyamide nanofilms toward better membrane selectivity,[9-11] such as co-solvent addition[12, 13] and nanofiller incorporation[14, 15]. For example, some studies applied co-solvents (e.g., acetone[16, 17] and ethyl acetate[18, 19]) to regulate the IP reaction to shape polyamide morphology[20] and/or tailor the crosslinking degree[21]. Some works incorporated porous metal-organic frameworks[22] and/or non-porous nanoparticles[23] during IP reaction to create selective channels toward high membrane performance. However, these strategies can suffer from some uncontrollable factors. For example, the volatility of co-solvents[20] and aggregation of nanofillers[23] can be inevitable, leading to their uncontrolled participance in IP. Besides, co-solvent toxicity and nanoparticle leaching can also harm the environment. Therefore, a facile and sustainable strategy to precisely control the IP reaction is desirable to effectively tailor polyamide properties toward better membrane selectivity.

Notably, polyamide polymerization is based on the reactive sites on monomers[24] (i.e., amino groups on PIP and acyl chloride groups on TMC). PIP shows strong nucleophilicity due to the lone pair electrons on the nitrogen atom of its amino groups. This can lead to the nucleophilic attack of PIP to the electron-deficient sites of acyl chlorides on TMC.[25] Highly reactive PIP molecules can continuously attack acyl chlorides during IP to form crosslinked polyamide.[24] According to the Henderson-Hasselbalch equation, PIP as a diacidic base with two pK_a values (pK_{a1} = 5.3 and pK_{a2} = 9.7)[26] can be protonated by H^+ to form mono- and di-protonated PIP at different pH.[27] Presumably, adjusting pH can effectively control the dominant monomer species in forms of non-, mono-, and di-protonated PIP, thereby influencing the reactivity of amine solution with TMC for the polyamide formation. Specifically, at a pH > pK_{a2}, the dominant non-protonated PIP with high reactivity can form the highly crosslinking degree of polyamide (**Figure 1**a). While at a lower pH, reduced non-protonated PIP with more protonated species can lead to less or ineffective crosslinked polyamide formation (**Figure 1**b and c). Indeed, several studies performed IP at different pH to tailor membrane performance.[28-31] However, the critical role of the pH-regulated reactive sites on PIP monomers in polyamide properties and membrane performance has not yet been systematically investigated.

Herein, we prepared polyamide NF membranes with varied pH values of amine solutions during IP. We hypothesize that the reactive sites on PIP could be effectively regulated by H^+ for polyamide formation with tailored properties. Due to the precise regulation, higher water permeance and better solute-solute selectivity were simultaneously achieved. Expectedly, this work using a facile paradigm provides insights into the role of the monomer reactive sites on membrane performance, paving

a novel direction for developing selective NF membranes toward diverse water treatment scenarios.

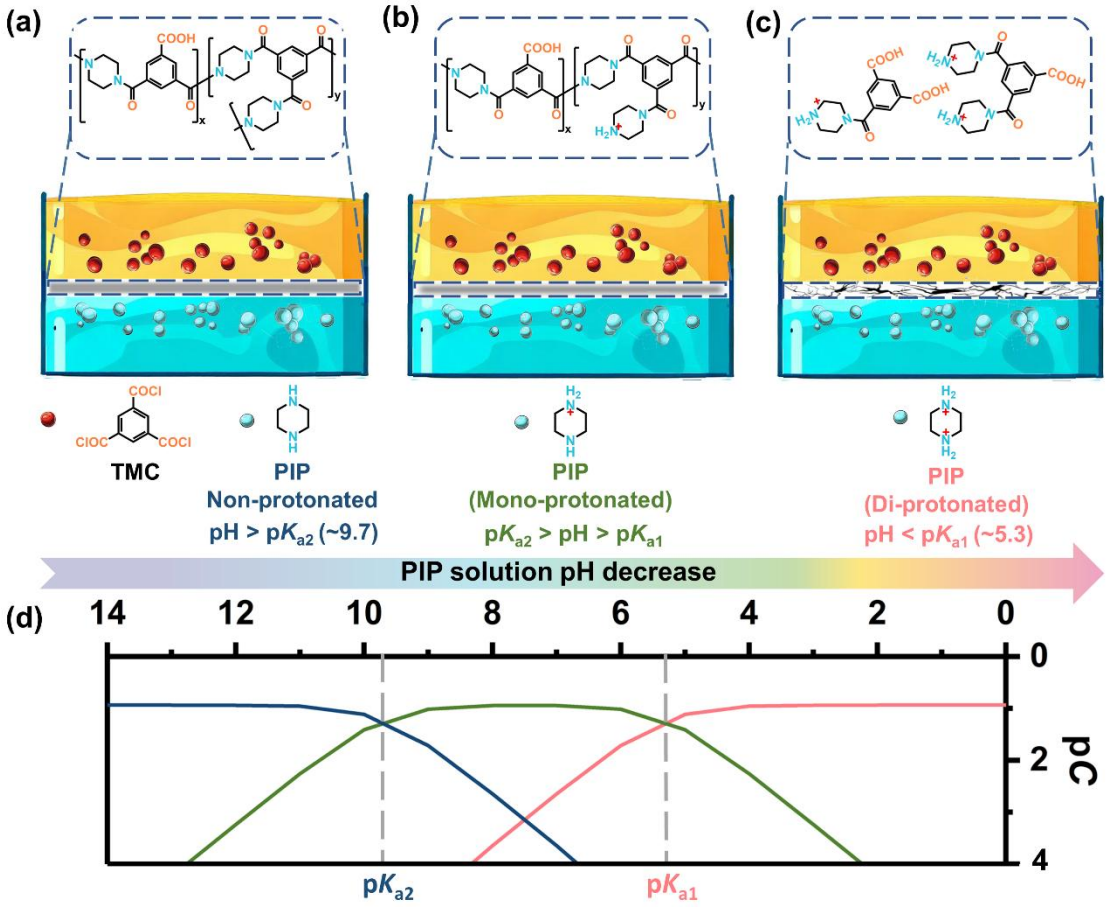

Figure 1. Schematic illustration of the dominant PIP species at different pH and corresponding interfacial polymerization. The formation of (a) highly crosslinked polyamide, (b) less crosslinked polyamide, and (c) ineffective crosslinked polyamide, at pH > pK_{a2} (non-protonated PIP is dominant), pK_{a1} < pH < pK_{a2} (mono-protonated PIP is dominant), and pH < pK_{a1} (di-protonated PIP is dominant), respectively. (d) The effect of pH on the different PIP species in amine solution. The total PIP concentration is 1.0 wt%. The pK_{a1} and pK_{a2} of PIP are 5.3 and 9.7, respectively (values obtained from reference[26]).

2. EXPERIMENTAL SECTION

2.1 Materials

Monomers piperazine (PIP, 99%, Sigma-Aldrich) and trimesoyl chloride (TMC, 98%, Sigma-Aldrich) were used for the IP reaction to form polyamide. n-Hexane (95%, Duksan) was used to dissolve TMC. Hydrochloride acid (HCl, VWR International) was applied to adjust the pH values of PIP solutions to fabricate pH-regulated NF membranes. The polyethersulfone (PES) ultrafiltration membrane (UP150) with a molecular weight cut-off (MWCO) of 150,000 Da, purchased from MICRODYN-NADIR, was used as the substrate in this study. The PES substrate was pre-treated with 25% (v/v) isopropanol/water solution for 1 h and then stored in deionized (DI) water before use. Sodium sulfate (Na_2SO_4, Dieckmann), sodium chloride (NaCl, Dieckmann), calcium chloride ($CaCl_2$, Dieckmann), and magnesium chloride ($MgCl_2$, Uni-Chem) were used to test the salt rejection of NF membranes. Glycerol (M.W. 93.12, Dieckmann), glucose (M.W. 180.16, Dieckmann), raffinose (M.W. 504.44, Sigma), and dextran (M.W. 1000, D-chem) were used to measure the MWCO of NF membranes. Anionic perfluoroalkyl substances, including perfluoro (2-methyl-3-oxahexanoic) acid (GenX, Macklin), potassium perfluorooctanesulfonate (PFOS, Sigma-Aldrich), perfluorobutyric acid (PFBA, Alfa Aesar), sodium perfluorooctanoate (PFOA, Alfa Aesar), and potassium nonafluoro-1-butanesulfonate (PFBS, TCI) were used for testing

micropollutant removal of NF membranes. Unless specified otherwise, the chemicals were dissolved in DI water for experiments.

2.2 Synthesis of NF Membranes

The NF membrane was fabricated via an IP reaction on a UP150 substrate (**Figure S1**).[32-34] In brief, a 1.0 wt% PIP solution with different regulated pH values (i.e., 10, 9, 8, and 7) was poured onto a UP150 substrate with an immersing time of 2 min. Then, the excessive PIP solution was removed with a rubber roller. Afterward, a 0.1 wt% TMC hexane solution was poured onto the PIP-impregnated substrate with a time of 1 min to produce the polyamide NF membrane. The fabricated membrane was rinsed by fresh n-hexane to clean off excess TMC and then stored in DI water before further use. These pH-regulated membranes were denoted as NF-pHx, where x represented the corresponding pH values of PIP solutions. The control membrane (denoted as NF-control) was formed by a 1.0 wt% PIP (pH 11.6, without pH regulation). We further adjusted the pH to 4 for the fabrication of ineffective crosslinked polyamide (denoted as NF-pH4)

2.3 Calculation of distribution coefficients for PIP species

The distribution coefficients of di-, mono-, and non-protonated PIP species in amine

solution (i.e., α_0, α_1, and α_2, respectively, see **Figure 1**d) can be specified as the fractions of corresponding PIP species over the total dissolved PIP molecules, which could be calculated by:

$$\alpha_0 = [H^+]^2/(K_{a1}K_{a2} + K_{a1}[H^+] + [H^+]^2) \quad (1)$$

$$\alpha_1 = K_{a1}[H^+]/(K_{a1}K_{a2} + K_{a1}[H^+] + [H^+]^2) \quad (2)$$

$$\alpha_2 = K_{a1}K_{a2}/(K_{a1}K_{a2} + K_{a1}[H^+] + [H^+]^2) \quad (3)$$

where K_{a1} and K_{a2} are the equilibrium constants of protonated PIP species. $[H^+]$ is the concentration of hydrogen ions in PIP solution, given as a pH value.

2.4 Characterization Methods

2.4.1 Morphology observation

Unless specified otherwise, membrane samples for all characterizations were dried in an oven with a temperature of 60 °C for 30 min. Field-emission scanning electron microscopy (FE-SEM, S-4800, Hitachi) was used for the surface morphology characterization of NF membranes. Before SEM characterization, a thin gold layer was sputter-coated onto the dried membrane samples to avoid charge accumulation.[35] Transmission electron microscopy (TEM, G2 20 Scanning, FEI Tecnai) was used for cross-section structure characterization of membrane samples.[36] Atomic force microscopy (AFM, Dimension Icon, Bruker) was used for the measurement of

membrane surface roughness with a 5.0×5.0 μm^2 scanning area.[37]

2.4.2 Chemical properties of NF membranes

Attenuated total reflection Fourier transform infrared spectroscopy (ATR FTIR, Nicolet iS5, Thermo Fisher Scientific) was conducted to analyze the polyamide formation.[16] A goniometer installed with a video capture device (OCA20, Dataphysics) was used to measure the water contact angles of dried membrane samples.[38] Streaming zeta potential (ζ) measurement tested by an electrokinetic analyzer (SurPASS 3, Anton Paar, Austria) was employed to analyze membrane surface charge in a pH range of 3.0-10.0 with 1.0 mM potassium chloride as the background solution.[16] X-ray photoelectron spectroscopy (XPS, Thermo Fisher Scientific, USA) with an X-ray source of Al- Kα gun was conducted to evaluate elemental compositions of membrane surface. The crosslinking degree of a typical PIP-based polyamide network could be calculated by the oxygen-to-nitrogen ratio (O/N) using the atomic percent of O and N:[35]

$$n = \frac{4-2r_{O/N}}{1+r_{O/N}} \quad (4)$$

where n is the crosslinking degree of polyamide and $r_{O/N}$ is the oxygen-to-nitrogen ratio obtained from XPS results.

2.5 Membrane Separation Performance

2.5.1 Water permeance and salt rejections

A cross-flow instrument was employed for membrane filtration experiments. The active filtration area of a membrane sample was 1×2 cm^2 and the operation temperature was 25 ± 1 °C. Before the sample collection for the tests of separation performance, the membrane coupon was stabilized under 5 bar for 1h. Then, the applied pressure was kept at 5 bar for the evaluation of water permeance and solute rejection. The water flux was calculated according to the following equation:

$$J_w = \frac{\Delta V}{\Delta t \times S} \quad (5)$$

where J_w (L m^{-2} h^{-1}) is the water flux, ΔV (L) is the permeate volume, Δt (h) is the sample collecting time, and S (m^2) is the effective membrane area. The water permeance was further calculated by the following equation:

$$A = \frac{J_w}{\Delta P - \Delta \pi} \quad (6)$$

where A (L m^{-2} h^{-1} bar^{-1}) is the water permeance, ΔP (bar) is the applied hydraulic pressure, and $\Delta \pi$ (bar) is the transmembrane pressure difference.

The salt rejection was measured using the feed solution with a single type of salt dissolved (1000 ppm Na_2SO_4, $MgCl_2$, $CaCl_2$, and NaCl), respectively. The MWCO experiment was performed by conducting the rejection tests of different neutral solutes

(200 ppm glycerol, glucose, raffinose, and dextran). The solute rejection was calculated according to the following equation:

$$R = \frac{C_f - C_p}{C_f} \quad (7)$$

where R is the solute rejection, C_f and C_p are the solute concentration of feed and permeate solution, respectively. A conductivity meter (Ultrameter II, Myron L Company, Carlsbad, CA) was applied to measure salt concentration. The concentration of neutral solutes was measured by a total organic carbon analyzer (TOC-L CPH, Shimadzu, Japan).

2.5.2 The analysis of polyamide pore size

According to previous literature,[32, 39] the rejection of these neutral solutes could be used to determine the pore size of polyamide. The distribution curve of polyamide pore size is presented as a log-normal distribution based on following assumptions: (1) the mean pore radius of polyamide membranes is equal to the radius of neutral solute molecular at 50% rejection; (2) the geometric standard deviation is defined as the ratio of solute radius at 84.13% rejection to that at 50% rejection; (3) there is no hydrodynamic or steric interaction between neutral solutes and polyamide pores.[11, 40] The mathematical expression for the distribution curve is given by:

$$\frac{dR(r_p)}{dr_p} = \frac{1}{r_p ln\sigma_p \sqrt{2\pi}} \exp\left[-\frac{(lnr_p - ln\mu_p)^2}{2(ln\sigma_p)^2}\right] \quad (8)$$

where r_p is the polyamide pore size, μ_p is the mean pore size, and σ_p is the geometric standard deviation of probability density function curve.

2.5.3 The rejection tests of contaminants by NF membranes

Anionic perfluoroalkyl substances, including PFOS, PFOA, GenX, PFBS, and PFBA, were applied to measure the rejection of contaminants by NF membranes. **Table S1** shows the physicochemical properties (e.g., structure formula and molecular weight) of these contaminants used in this work. Generally, these contaminants exist as anionic compounds under a circumneutral pH (~6.5) used for filtration tests. Before water sample collection, the testing membranes were compacted for 2 h with a feed solution consisting of PFOS, PFOA, GenX, PFBS, and PFBA (each with a concentration of 200 ppb) at an electrolyte background of 10 mM NaCl. The micropollutant concentration of feed and permeate solutions was tested by liquid chromatography with tandem mass spectrometry (LC-MS/MS, 1290 Infinity, Agilent; 3200 QTRAP, AB SCIEX, Singapore). The reversed-phase column (ZORBAX Eclipse Plus C18, Agilent) was 2.1×50 mm in dimension with the particle size of 1.8 μm. Details of contaminants analytical method can be referred in our previous work.[41]

2.5.4 The analysis of solute-to-solute selectivity

The solute-to-solute selectivity of NF membranes was evaluated according to the following equations:[42, 43]

$$S_{i/j} = \frac{1-R_i}{1-R_j} \quad (9)$$

where $S_{i/j}$ is the solute/solute selectivity of solute i over j (e.g., S_{CaCl_2/Na_2SO_4} represents the membrane selectivity between $CaCl_2$ and Na_2SO_4).

3. RESULTS AND DISCUSSIONS

3.1 Effectively Tailored Structure and Chemistry of NF Membranes

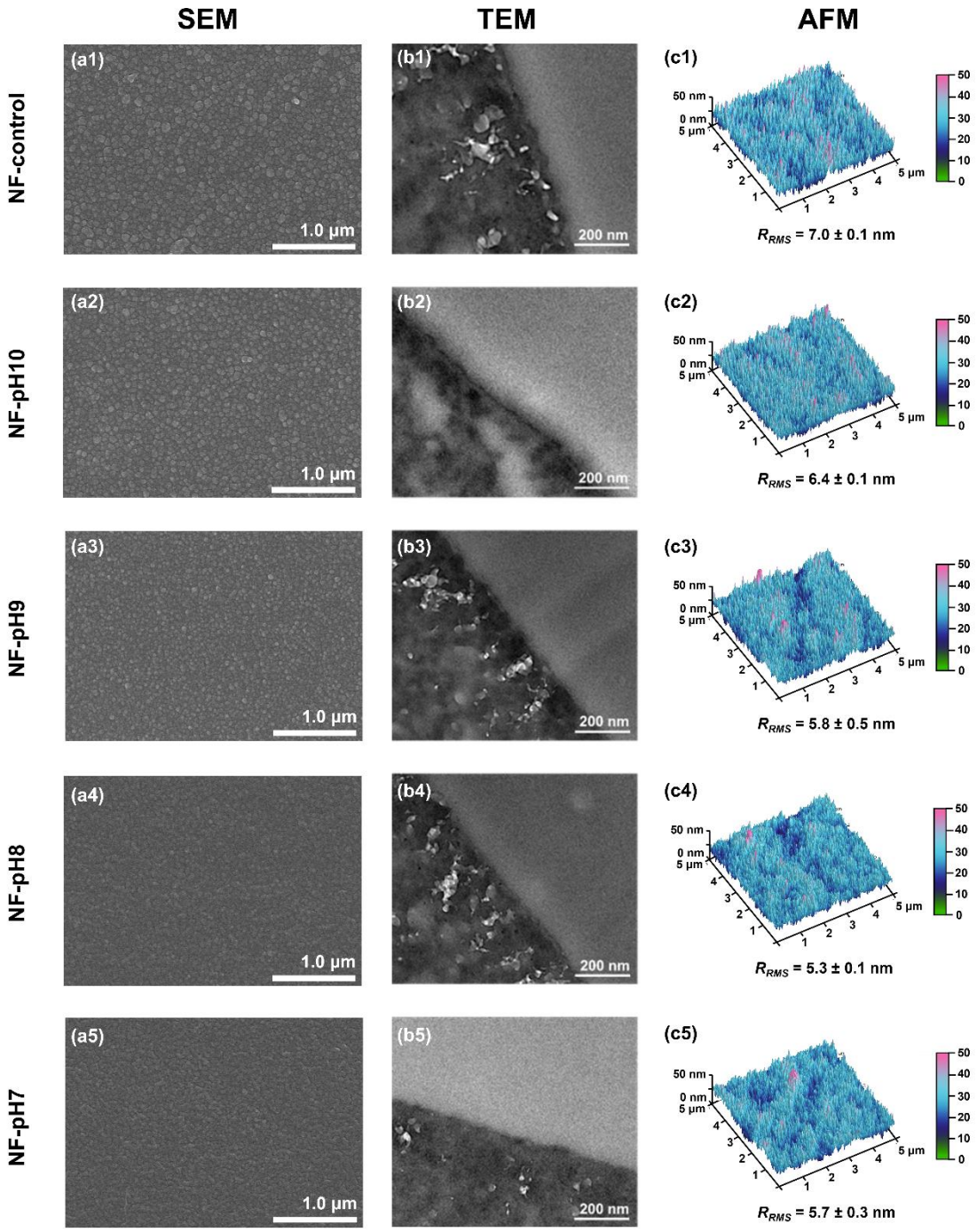

Figure 2. Micrographs of the polyamide surface morphology for NF membranes. (a1-a5) SEM top-viewed images. (b1-b5) TEM images. (c1-c5) AFM surface micrographs, where R_{RMS} is the root-mean-square surface roughness based on three independent tests.

Figure 2a shows the surface morphology of fabricated NF membranes (The SEM

image of UP150 substrate is shown in **Figure S3**). NF-control membrane, formed by PIP solution without pH adjustment, exhibited typical nodule-like surface nanofeatures[44] (**Figure 2**a1). The adjustment of PIP pH for IP reactions resulted in relatively smaller nodule-like nanofeatures on the membrane surface (**Figure 2**a2-a5). In addition, general trends of lower surface roughness (i.e., R_{RMS} obtained from AFM micrographs, **Figure 2**c) and reduced polyamide thickness (obtained from TEM micrographs, **Figure 2**b) were observed for NF membranes formed at lower pHs. These observations can be attributed to the varied dominant PIP species from the non-protonated (pH > pK_{a2} of 9.7) to the protonated (pH < pK_{a2}) (**Figure 1**d). Specifically, the non-protonated PIP is highly reactive, which could trigger a relatively violent IP reaction for the polyamide formation[25, 45] of NF-control (i.e., pH 11.6) and NF-pH10 membranes. Decreasing the pH values below pK_{a2} resulted in a reduced fraction of highly reactive non-protonated PIP while an increased fraction of less reactive protonated species. This can lead to the lower reactivity of amine solution, which can slow down the IP reaction rate [25, 45] and thus form the relatively smaller surface nanofeatures and smoother surface morphology.[46]

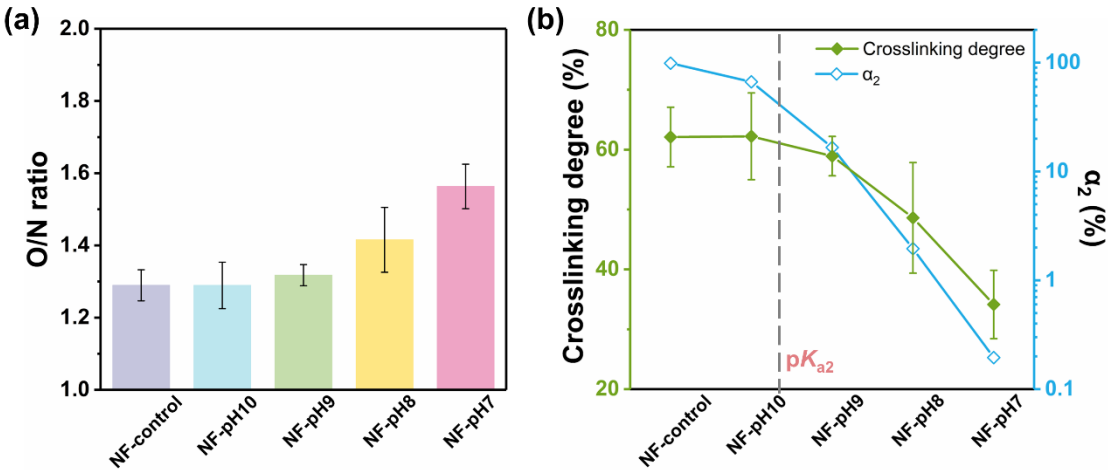

Figure 3. Polyamide physicochemical properties of NF membranes. (a) The ratio of oxygen to nitrogen (O/N ratio). The O/N ratio is calculated based on XPS results from at least three independent experiments. (b) Crosslinking degree of polyamide membranes based on at least three parallel measurements. α_2 is the distribution coefficient of non-protonated PIP (i.e., the fraction of non-protonated PIP over total dissolved PIP) in aqueous solution calculated based on Eq. 3.

Generally, the O/N ratio based on XPS surface analysis increased from 1.29 for NF-control to 1.56 for NF-pH7 membrane (**Figure 3**a), corresponding to a decreased crosslinking degree from 62% to 34% (**Figure 3**b). This trend of crosslinking degree was consistent with the reduced distribution coefficient (α_2) of non-protonated PIP (i.e., the fraction of non-protonated PIP) (**Figure 3**b), implying the critical role of the fraction of highly reactive PIP in polyamide formation. At pH > pK_{a2} (i.e., NF-control and NF-pH10 membranes), non-protonated PIP is the dominant species in the amine solution (**Figure 1**d). These PIP molecules with high reactivity could lead to highly crosslinked polyamide (**Figure 1**a). In contrast, decreasing the amine pH below pK_{a2} led to less crosslinked polyamide (**Figure 1**b), which can be due to the reduced α_2 accompanied by more mono-protonated species (**Figure 1**d). Further decreasing amine pH below

pK_{a1} resulted in ineffective crosslinked polyamide, as indicated by XPS results (**Table S3**). This could be attributed to the dominant di-protonated PIP with few non-protonation. Lower crosslinking degree often leads to a relatively looser polyamide structure with a larger pore size.[47] For example, the NF-pH8 membrane possessed a larger MWCO (around 500) than that (around 180) of the NF-control membrane (**Figure S6**), indicating its larger pore size. The pore size of membranes can be calculated according to the rejection value based on the log-normal distribution assumption. The estimated mean pore radius of NF-control and NF-pH8 was 0.28 nm and 0.38 nm, respectively (**Figure 4**a). In addition, less crosslinked polyamide features more residual acyl chlorides, which can be hydrolyzed to enhance the negative charge of polyamide surface. Consistently, the zeta potential values of the NF-pH8 membrane were generally lower than those of the NF-control membrane (**Figure 4**b). In respect to the other surface properties, these NF membranes possessed similar water contact angles (around 90°, **Figure S5**) and characteristic FTIR peaks (1620 cm^{-1} for amide group, **Figure S2**).

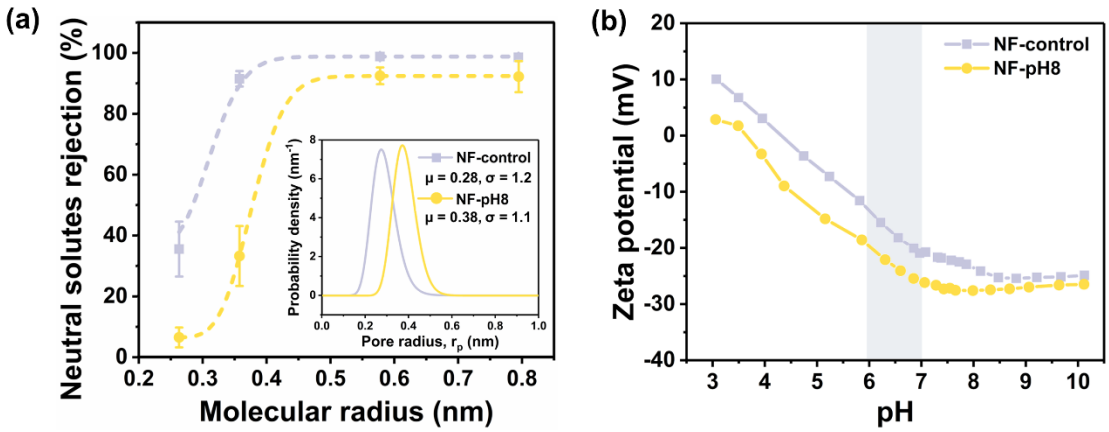

Figure 4. (a) Neutral solute (i.e., glycerol, glucose, raffinose, and dextran) rejections with different molecular weights (93.12, 180.16, 504.44, and 1000 Da) for NF-control and NF-pH8 membranes. The filtration tests of neutral solutes were repeated at least three times. The dash lines are established based on the log-normal distribution of membrane pore size. Inset is the pore size distribution of NF membranes estimated by neutral solutes rejection results. The mean pore radius and geometric standard deviation are also annotated. (b) Zeta potential analysis of NF-control and NF-pH8 membranes. Generally, the higher MWCO represents the larger mean effective pore size of polyamide.[8]

3.2 Membrane Separation Performance

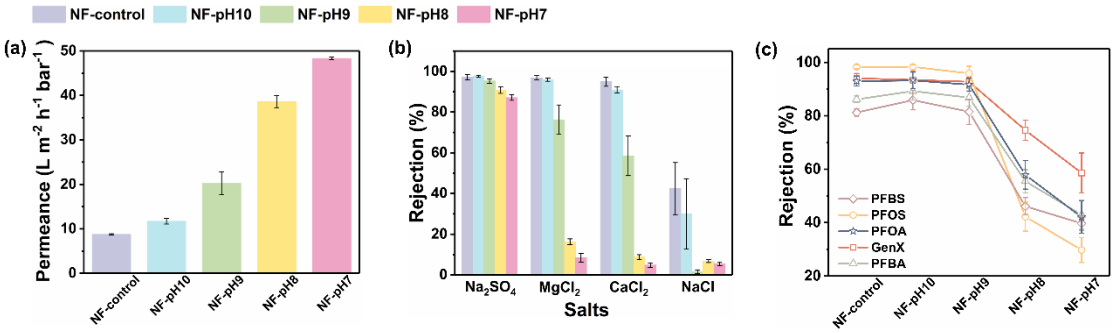

Figure 5. The separation performance of NF membranes. (a) Pure water permeance, (b) rejection of four salts, and (c) rejection of micropollutants. Filtration experiment conditions: applied hydraulic pressure is 5 bar and temperature is 25 °C. The membrane rejection of four salts was analyzed by the feed solution with a single type of salt dissolved (1000 ppm Na_2SO_4, $MgCl_2$, $CaCl_2$, and NaCl), respectively. The rejection test of micropollutants was conducted using a mixed solution containing 5 anionic perfluoroalkyl substances with a concentration of 200 ppb for each. All the results were based on at least three parallel measurements.

Generally, decreasing PIP pH for polyamide formation resulted in improved water

permeance of NF membranes (**Figure 5**a). For the control and NF-pH10 membranes, their water permeance was relatively lower. For other membranes formed at pH < pK_{a2}, the membrane permeance was significantly improved, up to 48.3 ± 0.3 L m^{-2} h^{-1} bar^{-1} of the NF-pH7 membrane. This significant improvement could be attributed to the obvious reduction of polyamide crosslinking degree at pH < pK_{a2} (**Figure 3**b) and thinner polyamide layer (**Figure 2**b), which could greatly reduce the water transport resistance across the membrane.

All these NF membranes exhibited relatively high rejections of Na_2SO_4 (over 87%) while their rejections of NaCl were generally lower than 40% (**Figure 5**b). This can be attributed to the combined effects of size exclusion and charge repulsion.[2, 47] NF membranes possessed stronger size exclusion for SO_4^{2-} than Cl^- due to the larger hydraulic radius of SO_4^{2-}. Besides, these membranes also gave enhanced electrostatic repulsion to divalent SO_4^{2-} than monovalent Cl^- by their negatively charged surfaces. Interestingly, the significantly reduced rejection of $CaCl_2$ was observed from 95% of NF-control to 5% of NF-pH7. A similar trend for the rejection of $MgCl_2$ was also observed (**Figure 5**b). These greatly reduced rejections of divalent cations could be attributed to the reduced crosslinking degree of polyamide formed at pH < pK_{a2}. The less crosslinked polyamide generally features a looser structure for weakened size

exclusion and more negative charge for enhanced charge interaction.[47] Both facilitate the passage of $CaCl_2$ and $MgCl_2$. In addition, the membrane formed at pH < pK_{a1} (i.e., NF-pH4) gave negligible salt rejection (e.g., 0.9 ± 0.3 % for Na_2SO_4 and 0.7 ± 0.3 % for $CaCl_2$) (**Table S3**) due to its ineffective-crosslinked polyamide. Furthermore, the rejection of micropollutants was reduced at lower pH (**Figure 5**c), which could be explained by the weakened size exclusion[48] resulting from the reduced crosslinking degree of polyamide (**Figure 3**b).

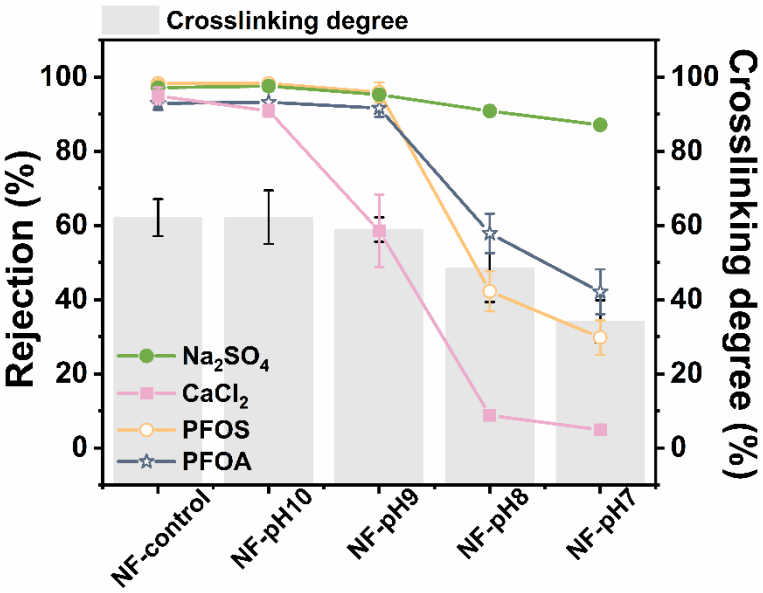

Figure 6. The rejection performance of Na_2SO_4, $CaCl_2$, PFOS, and PFOA by NF membranes. Na_2SO_4 and perfluoroalkyl substances (i.e., PFOS and PFOA) represent the divalent and monovalent anions, respectively. $CaCl_2$ represents the divalent cations. The rejection of Na_2SO_4 and $CaCl_2$ was measured using the feed solution with a single type of salt dissolved. The rejection of anionic perfluoroalkyl substances was measured with a feed solution containing a cocktail of PFOS, PFOA, GenX, PFBS, and PFBA in a NaCl background solution.

Generally, the solute rejection is influenced by the combined effects of size exclusion

and charge interaction.[2, 8] To better elucidate the underlying rejection mechanisms, we compared the rejection performance of several solutes and polyamide crosslinking degree for these NF membranes (**Figure 6**). For the rejection of anions (i.e., Na_2SO_4, PFOS, and PFOA), disparate trends were observed. Specifically, the rejection of Na_2SO_4 remained high (87-97%). In contrast, the rejection of monovalent anionic PFOS and PFOA remained around 90% at pH ≥ 9 and then decreased greatly at lower pH. This different rejection performance could be attributed to the competing effects of size exclusion and charge repulsion. As shown in **Figure 3** and **4**, decreasing the pH of the PIP solution weakens the size exclusion effect (due to increased membrane pore size) but enhances the charge interaction (due to the more negative membrane surface charge). In addition, the charge repulsion between divalent SO_4^{2-} and negative polyamide was stronger compared to that between monovalent anions (PFOA and PFOS) and polyamide.[47, 48] For membranes formed at lower pH, the enhanced charge repulsion of Na_2SO_4 could play a dominant role to offset the weakened size exclusion effect, thereby maintaining high rejection. In contrast, the enhancement effect for charge repulsion is less pronounced for the monovalent anions PFOA and PFOS, which is less effective in offsetting the reduced size exclusion, leading to decreased rejection of these compounds at lower pH. For the divalent cations ($CaCl_2$), the rejection dramatically decreased from 95% to 5%. This sharp reduction can be explained by the

synergic effects of looser structure and more negative charge on the passage of divalent Ca^{2+} through the membrane.

3.3 Tailored Solute-to-Solute Selectivity of NF membranes

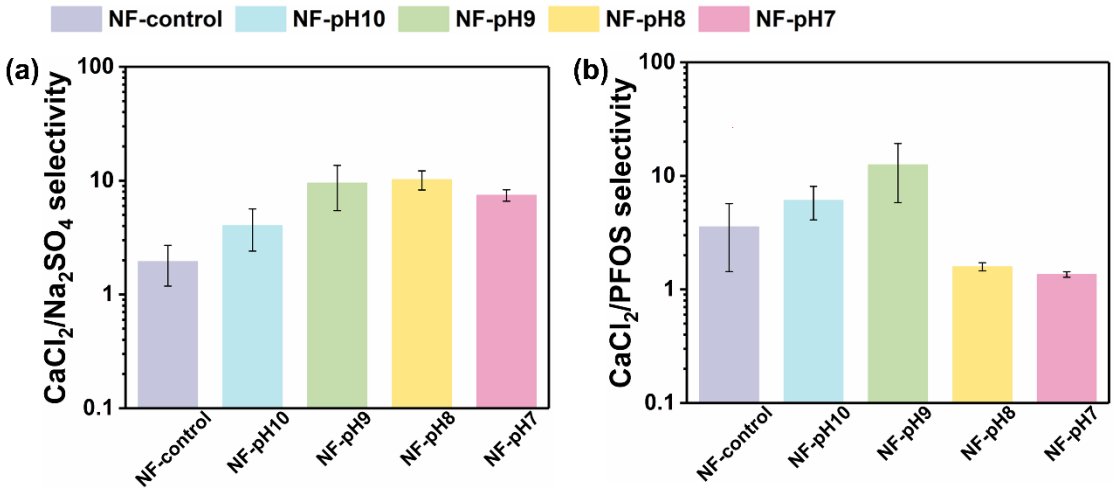

Figure 7. The solute-to-solute selectivity of NF membranes: (a) $CaCl_2/Na_2SO_4$ and (b) $CaCl_2$/PFOS. The membrane selectivity is calculated based on the solute rejection.

Our results indicated that tailoring reactive sites on PIP by varying the dominant amine species could effectively regulate polyamide crosslinking degree to influence the rejection to different solutes. **Figure 7** and **Figure S7** further present different solute-to-solute selectivity. Generally, decreasing pH significantly improved $CaCl_2/Na_2SO_4$ selectivity up to 10 (for NF-pH8), which was an order of magnitude higher than that of the NF-control membrane (**Figure 7**a). This significant improvement in membrane selectivity was attributed to the greatly reduced rejection of $CaCl_2$ and maintained high rejection of Na_2SO_4 (**Figure 6**). To further evaluate the NF membranes in this study, we

also included a benchmark in the form of an upper bound plot of $CaCl_2/Na_2SO_4$ selectivity vs. water permeance based on the performance data of NF membranes reported in literature (**Figure 8**). NF-pH8 and NF-pH9 in this study showed comparable or even better $CaCl_2/Na_2SO_4$ selectivity compared to many other membranes. In addition, the selectivity of $CaCl_2$/PFOS was increased up to 12 (for NF-pH9), which was 3.5 times higher than that of the control membrane (**Figure 7**b). This obvious enhancement was attributed to the different rejection performance between $CaCl_2$ and PFOS (**Figure 6**).

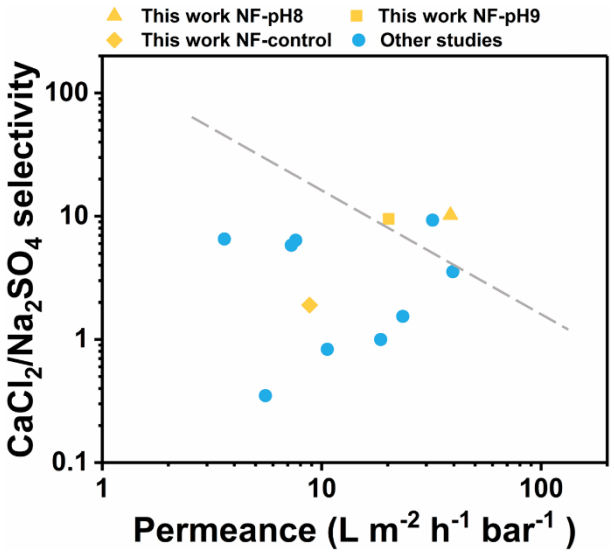

Figure 8. Comparison of $CaCl_2/Na_2SO_4$ selectivity for prepared NF membranes vs. recent NF membranes in literature. Their specific separation performance data are shown in **Table S4**.

In the NF literature, it is commonly believed that the water permeance and solute-to-solute selectivity are key indicators to evaluate the membrane performance for

applications.[1] Here, we demonstrated the potential of tailoring PIP reactive sites to simultaneously enhance water permeance and membrane selectivity. To be noted, the choice of optimal membrane is greatly influenced by the specific application. For example, the NF-pH8 membrane featuring high $CaCl_2/Na_2SO_4$ selectivity (**Figure 7**a) could be applied for the desalination pretreatment to avoid scaling issue.[30] For the environmental applications involved in contaminant removal (e.g., PFOS removal from contaminated groundwater), the NF-pH9 membrane could be a better candidate due to its high rejection of contaminants (**Figure 5**c) and enhanced mineral/contaminant selectivity[48] (**Figure 7**b). For example, in the context of drinking water treatment, Ca^{2+} is crucial for human health. Therefore, enough minerals (i.e., low rejection to Ca^{2+}) are crucial for high-quality drinking water production in addition to high PFOS rejection.[34]

4. Conclusions

This study clarified that the pH regulation of amine solution for varied PIP reactive sites can effectively control polyamide properties toward enhanced membrane performance. The less crosslinked polyamide was formed at pH values between the two pK_a values (i.e., 5.3 and 9.7, respectively) of the diacidic base PIP, where mono-protonated PIP is dominant with the reduced fraction of non-protonated species. Such polyamide featured looser structure and more negative charge compared to the highly crosslinked NF-control formed at pH > pK_{a2}. The looser structure facilitated water transport through polyamide to significantly improve the water permeance (e.g., over 4 times higher than that of NF-control). Meanwhile, the more negative charge enhanced charge repulsion to anions and charge attraction to cations, leading to significantly higher solute-to-solute selectivity (e.g., an order of magnitude higher $CaCl_2/Na_2SO_4$ selectivity). These results suggested that precise regulation of monomer reactive sites could be a promising strategy to enhance water permeance and membrane selectivity of polyamide NF membranes. Future studies would further investigate if the reactive sites and monomer species could be regulated by other factors. Our work proposed a facile strategy to tailor the polyamide properties and membrane performance, providing novel insights into the future design and development of selective NF membranes toward diverse application scenarios.

ASSOCIATED CONTENT

Supporting Information

The Supporting Information is available free of charge at

Section S1, Synthesis of NF membranes; Section S2, Physicochemical properties of anionic perfluoroalkyl substances; Section S3, Characterization results; Section S4, Membrane selectivity.

AUTHOR INFORMATION

Corresponding Authors

Chuyang Y. Tang – Department of Civil Engineering, The University of Hong Kong, Hong Kong 999077, P. R. China; ORCID 0000-0002-7932-6462; Tel: +852-2859 1976; E-mail address: tangc@hku.hk

Li Long – Department of Civil Engineering, The University of Hong Kong, Hong Kong 999077, P. R. China; ORCID 0000-0002-7951-3276; Tel: +852-6740 2649; E-mail address: longli@connect.hku.hk

Authors

Ke Jiang – Department of Civil Engineering, The University of Hong Kong, Hong Kong 999077, P. R. China; ORCID 0000-0002-8077-5951

Lu Elfa Peng – Department of Civil Engineering, The University of Hong Kong, Hong Kong 999077, P. R. China; ORCID 0000-0002-3223-4608

Zhe Yang – Department of Civil Engineering, The University of Hong Kong, Hong Kong 999077, P. R. China; ORCID 0000-0003-0753-3902

Wenyu Liu –Department of Civil Engineering, The University of Hong Kong, Hong Kong 999077, P. R. China; ORCID 0000-0003-3298-8191

Dong-Myeong Shin – Department of Mechanical Engineering, The University of Hong Kong, Hong Kong 999077, P. R. China; ORCID 0000-0002-5402-9947

Notes

The authors declare no competing financial interest.

ACKNOWLEDGEMENTS

This work was financially supported by the Guangdong-Hong Kong Technology Cooperation Funding Scheme (GHP/181/20GD) under the Innovation and Technology Fund of Hong Kong Special Administration Region of China and Science and Technology Planning Project of Guangdong Province (2021A0505110013). Lu Elfa Peng is supported by an RGC Postdoctoral Fellowship from the Research Grants Council of the Hong Kong Special Administration Region, China (PDFS2223-7S02). The Electron Microscope Unit at HKU is thanked for assisting SEM characterization.

REFERENCES

(1) Mohammad, A. W.; Teow, Y. H.; Ang, W. L.; Chung, Y. T.; Oatley-Radcliffe, D. L.; Hilal, N. Nanofiltration membranes review: Recent advances and future prospects. *Desalination* **2015**, *356*, 226-254.

(2) Wang, K.; Wang, X.; Januszewski, B.; Liu, Y.; Li, D.; Fu, R.; Elimelech, M.; Huang, X. Tailored design of nanofiltration membranes for water treatment based on synthesis-property-performance relationships. *Chem. Soc. Rev.* **2022**, *51* (2), 672-719.

(3) Gohil, J. M.; Ray, P. A review on semi-aromatic polyamide TFC membranes prepared by interfacial polymerization: Potential for water treatment and desalination.

Sep. Purif. Technol. **2017**, *181*, 159-182.
(4) Ismail, A. F.; Padaki, M.; Hilal, N.; Matsuura, T.; Lau, W. J. Thin film composite membrane — Recent development and future potential. *Desalination* **2015**, *356*, 140-148.
(5) Freger, V.; Ramon, G. Z. Polyamide desalination membranes: Formation, structure, and properties. *Prog. Polym. Sci.* **2021**, *122*, 101451.
(6) Lu, X.; Elimelech, M. Fabrication of desalination membranes by interfacial polymerization: history, current efforts, and future directions. *Chem. Soc. Rev.* **2021**, *50* (11), 6290-6307.
(7) Park, H. B.; Kamcev, J.; Robeson, L. M.; Elimelech, M.; Freeman, B. D. Maximizing the right stuff: The trade-off between membrane permeability and selectivity. *Science* **2017**, *356* (6343), eaab0530.
(8) Zhang, H.; He, Q.; Luo, J.; Wan, Y.; Darling, S. B. Sharpening nanofiltration: strategies for enhanced membrane selectivity. *ACS Appl. Mater. Interfaces* **2020**, *12* (36), 39948-39966.
(9) Porter, C. J.; Wang, L.; Zhong, M.; Elimelech, M. Tuning charge density in tethered electrolyte active-layer membranes for enhanced ion-ion selectivity. *J. Membr. Sci.* **2023**, *668*, 121214.
(10) Liu, J.; Hua, D.; Zhang, Y.; Japip, S.; Chung, T. S. Precise molecular sieving architectures with janus pathways for both polar and nonpolar molecules. *Adv. Mater.* **2018**, *30* (11), 1705933.
(11) Liang, Y.; Zhu, Y.; Liu, C.; Lee, K. R.; Hung, W. S.; Wang, Z.; Li, Y.; Elimelech, M.; Jin, J.; Lin, S. Polyamide nanofiltration membrane with highly uniform sub-nanometre pores for sub-1 Å precision separation. *Nat. Commun.* **2020**, *11* (1), 2015.
(12) Sun, Y.; Zhong, J.; Lin, Z.; Sun, R.; Chen, L.; Jiang, Z.; Pang, J. Rigid twisted structured PA membranes for organic solvent nanofiltration via co-solvent assisted interfacial polymerization. *J. Membr. Sci.* **2023**, *666*, 121179.
(13) Fu, W.; Deng, L.; Hu, M.; Mai, Z.; Xu, G.; Shi, Y.; Guan, K.; Gonzales, R. R.; Matsuoka, A.; Matsuyama, H. Polyamide composite membrane with 3D honeycomb-like structure via acetone-regulated interfacial polymerization for high-efficiency organic solvent nanofiltration. *J. Membr. Sci.* **2023**, *679*, 121711.
(14) Zhao, Y.; Tong, T.; Wang, X.; Lin, S.; Reid, E. M.; Chen, Y. Differentiating solutes with precise nanofiltration for next generation environmental separations: A review. *Environ. Sci. Technol.* **2021**, *55* (3), 1359-1376.
(15) Wu, X.; Shaibani, M.; Smith, S. J. D.; Konstas, K.; Hill, M. R.; Wang, H.; Zhang, K.; Xie, Z. Microporous carbon from fullerene impregnated porous aromatic frameworks for improving the desalination performance of thin film composite forward osmosis membranes. *J. Mater. Chem. A* **2018**, *6* (24), 11327-11336.

(16) Gan, Q.; Peng, L. E.; Guo, H.; Yang, Z.; Tang, C. Y. Cosolvent-sssisted interfacial polymerization toward regulating the morphology and performance of polyamide reverse osmosis membranes: Increased m-phenylenediamine solubility or enhanced interfacial vaporization? *Environ. Sci. Technol.* **2022**, *56* (14), 10308-10316.
(17) Hailemariam, R. H.; Choi, J.-S.; Damtie, M. M.; Rho, H.; Park, K.-D.; Lee, J.; Woo, Y. C. Enhancing performances of polyamide thin film composite membranes via co-solvent assisted interfacial polymerization. *Desalination* **2022**, *524*, 115481.
(18) Li, C.; Zhao, Y.; Lai, G. S.; Wang, R. Investigation of aqueous and organic co-solvents roles in fabricating seawater reverse osmosis membrane. *J. Membr. Sci.* **2022**, *645*, 120187.
(19) Kamada, T.; Ohara, T.; Shintani, T.; Tsuru, T. Optimizing the preparation of multi-layered polyamide membrane via the addition of a co-solvent. *J. Membr. Sci.* **2014**, *453*, 489-497.
(20) Peng, L. E.; Jiang, Y.; Wen, L.; Guo, H.; Yang, Z.; Tang, C. Y. Does interfacial vaporization of organic solvent affect the structure and separation properties of polyamide RO membranes? *J. Membr. Sci.* **2021**, *625*, 119173.
(21) Wang, Y.; Chang, H.; Jiang, S.; Chen, J.; Wang, J.; Liang, H.; Li, G.; Tang, X. An efficient co-solvent tailoring interfacial polymerization for nanofiltration: enhanced selectivity and mechanism. *J. Membr. Sci.* **2023**, *677*, 121615.
(22) Dai, R.; Guo, H.; Tang, C. Y.; Chen, M.; Li, J.; Wang, Z. Hydrophilic selective nanochannels created by metal organic frameworks in nanofiltration membranes enhance rejection of hydrophobic endocrine-disrupting compounds. *Environ. Sci. Technol.* **2019**, *53* (23), 13776-13783.
(23) Yang, Z.; Huang, X.; Ma, X.-h.; Zhou, Z.-w.; Guo, H.; Yao, Z.; Feng, S.-P.; Tang, C. Y. Fabrication of a novel and green thin-film composite membrane containing nanovoids for water purification. *J. Membr. Sci.* **2019**, *570-571*, 314-321.
(24) Montalbetti, C. A. G. N.; Falque, V. Amide bond formation and peptide coupling. *Tetrahedron* **2005**, *61* (46), 10827-10852.
(25) Palling, D.; Jencks, W. P. Nucleophilic reactivity toward acetyl chloride in water. *J. Am. Chem. Soc.* **1984**, *106* (17), 4869-4876.
(26) Lide, D. R. *CRC handbook of chemistry and physics*; CRC press: Boca Raton, 2004.
(27) Bishnoi, S.; Rochelle, G. T. Absorption of carbon dioxide into aqueous piperazine: reaction kinetics, mass transfer and solubility. *Chem. Eng. Sci.* **2000**, *55* (22), 5531-5543.
(28) Gao, Y.; Wang, X.-m.; Huang, X. The veiled impacts of H^+ on interfacial polymerization and its effects on nanofiltration performance. *Environ. Sci. Technol. Lett.* **2023**, *10* (3), 274-279.

(29) Zhao, C.; Zhang, Y.; Jia, Y.; Li, B.; Tang, W.; Shang, C.; Mo, R.; Li, P.; Liu, S.; Zhang, S. Polyamide membranes with nanoscale ordered structures for fast permeation and highly selective ion-ion separation. *Nat. Commun.* **2023**, *14* (1), 1112.
(30) Yang, W.; Long, L.; Guo, H.; Wu, C.; Zhou, S.; Mei, Y.; Peng, L. E.; Liu, W.; Yang, Z.; Li, W.; et al. Facile synthesis of nanofiltration membrane with asymmetric selectivity towards enhanced water recovery for groundwater remediation. *J. Membr. Sci.* **2022**, *663*, 121038.
(31) Zhu, X.; Cheng, X.; Luo, X.; Liu, Y.; Xu, D.; Tang, X.; Gan, Z.; Yang, L.; Li, G.; Liang, H. Ultrathin thin-film composite polyamide membranes constructed on hydrophilic poly(vinyl alcohol) decorated support toward enhanced nanofiltration performance. *Environ. Sci. Technol.* **2020**, *54* (10), 6365-6374.
(32) Nghiem, L. D.; Schafer, A. I.; Elimelech, M. Removal of natural hormones by nanofiltration membranes: measurement, modeling, and mechanisms. *Environ. Sci. Technol.* **2004**, *38* (6), 1888-1896.
(33) Lv, Y.; Du, Y.; Qiu, W. Z.; Xu, Z. K. Nanocomposite membranes via the codeposition of polydopamine/polyethylenimine with silica nanoparticles for enhanced mechanical strength and high water permeability. *ACS Appl. Mater. Interfaces* **2017**, *9* (3), 2966-2972.
(34) Wang, T.; Han, H.; Wu, Z.; Dai, R.; Wang, Z. Humic acid modified selective nanofiltration membrane for efficient separation of PFASs and mineral salts. *ACS ES&T Water* **2022**, *2* (6), 1152-1160.
(35) Peng, L. E.; Yao, Z.; Liu, X.; Deng, B.; Guo, H.; Tang, C. Y. Tailoring polyamide rejection layer with aqueous carbonate chemistry for enhanced membrane separation: mechanistic insights, chemistry-structure-property relationship, and Environmental Implications. *Environ. Sci. Technol.* **2019**, *53* (16), 9764-9770.
(36) Zhou, S.; Long, L.; Yang, Z.; So, S. L.; Gan, B.; Guo, H.; Feng, S. P.; Tang, C. Y. Unveiling the growth of polyamide nanofilms at water/organic free interfaces: Toward enhanced water/salt selectivity. *Environ. Sci. Technol.* **2022**, *56* (14), 10279-10288.
(37) Gan, Q.; Wu, C.; Long, L.; Peng, L. E.; Yang, Z.; Guo, H.; Tang, C. Y. Does surface roughness necessarily increase the fouling propensity of polyamide reverse osmosis membranes by humic acid? *Environ. Sci. Technol.* **2023**, *57* (6), 2548-2556.
(38) Guo, H.; Yao, Z.; Wang, J.; Yang, Z.; Ma, X.; Tang, C. Y. Polydopamine coating on a thin film composite forward osmosis membrane for enhanced mass transport and antifouling performance. *J. Membr. Sci.* **2018**, *551*, 234-242.
(39) Xie, M.; Nghiem, L. D.; Price, W. E.; Elimelech, M. Relating rejection of trace organic contaminants to membrane properties in forward osmosis: measurements, modelling and implications. *Water Res.* **2014**, *49*, 265-274.
(40) Zhang, S.; Fu, F.; Chung, T.-S. Substrate modifications and alcohol treatment on

thin film composite membranes for osmotic power. *Chem. Eng. Sci.* **2013**, *87*, 40-50.
(41) Guo, H.; Wang, J.; Han, Y.; Feng, Y.; Shih, K.; Tang, C. Y. Removal of perfluorooctane sulfonate by a gravity-driven membrane: Filtration performance and regeneration behavior. *Sep. Purif. Technol.* **2017**, *174*, 136-144.
(42) Zhang, L.; Zhang, R.; Ji, M.; Lu, Y.; Zhu, Y.; Jin, J. J. J. o. M. S. Polyamide nanofiltration membrane with high mono/divalent salt selectivity via pre-diffusion interfacial polymerization. *J. Membr. Sci.* **2021**, *636*, 119478.
(43) Li, P.; Lan, H.; Chen, K.; Ma, X.; Wei, B.; Wang, M.; Li, P.; Hou, Y.; Jason Niu, Q. Novel high-flux positively charged aliphatic polyamide nanofiltration membrane for selective removal of heavy metals. *Sep. Purif. Technol.* **2022**, *280*, 119949.
(44) Zhu, B.; Shao, R.; Li, N.; Guo, C.; Liu, P.; Shi, J.; Min, C.; Liu, S.; Qian, X.; Wang, L.; et al. Narrowing the pore size distribution of polyamide nanofiltration membranes via dragging piperazines to enhance ion selectivity. *J. Membr. Sci.* **2023**, *667*, 121187.
(45) Zhang, L.; Wang, X.-j.; Wang, J.; Grinberg, N.; Krishnamurthy, D.; Senanayake, C. H. An improved method of amide synthesis using acyl chlorides. *Tetrahedron Lett.* **2009**, *50* (24), 2964-2966.
(46) Lai, C.; Zhu, X.; Li, J.; Zhou, W.; Xu, J.; Ding, J.; Song, J.; Wu, D.; Liang, H.; Cheng, X. pH-regulated interfacially polymerized nanofiltration membranes to achieve high separation of NOM and moderate desalination for purifying ground water. *Desalination* **2022**, *544*, 116148.
(47) Liu, Z.; Zhao, L.; Ye, H.; Wang, Z.; Chen, Y.; Li, Y.; Liu, L.; Guo, Y.; Chen, Y.; Niu, Q. J. Highly anions-selective polyamide nanofiltration membrane fabricated by rod-coating assisted interfacial polymerization. *J. Membr. Sci.* **2023**, *668*, 121273.
(48) Guo, H.; Dai, R.; Xie, M.; Peng, L. E.; Yao, Z.; Yang, Z.; Nghiem, L. D.; Snyder, S. A.; Wang, Z.; Tang, C. Y. Tweak in puzzle: Tailoring membrane chemistry and structure toward targeted removal of organic micropollutants for water reuse. *Environ. Sci. Technol. Lett.* **2022**, *9* (4), 247-257.